

Competing growth kinetics in simultaneously crystallizing and phase-separating polymer blends

Howard Wang,^{a)} Katsumi Shimizu, Hongdoo Kim,^{b)} Erik K. Hobbie, Zhi-Gang Wang, and Charles C. Han

Polymers Division, National Institute of Standards and Technology, Gaithersburg, Maryland 20899

(Received 1 August 2001; accepted 4 February 2002)

The kinetic interplay between crystal superstructure growth and late-stage liquid phase coarsening in a polymer blend has been examined. By controlling the relative quench depths for liquid–liquid phase separation and crystallization, the growth kinetics of the characteristic length scales of the simultaneous ordering processes show a crossover from crystallization dominated to phase-separation dominated behavior. Based on a scaling argument for late-stage coarsening during spinodal decomposition, we argue that this kinetic crossover is inevitable in a blend for which the critical temperature of liquid–liquid phase separation is well above the equilibrium melting temperature of the blend. © 2002 American Institute of Physics. [DOI: 10.1063/1.1464537]

INTRODUCTION

Although critical phenomena and phase separation in binary mixtures have been well studied and are reasonably well understood, the complexity of the interplay between liquid–liquid phase separation (LLPS) and another phase transition such as crystallization remains largely unexplored.¹ In a binary liquid mixture in which one component crystallizes upon cooling, a quantitative understanding of the kinetics of the simultaneous ordering processes of solidification and macroscopic phase separation has yet to be achieved. For example, both LLPS and crystallization of polymers have been studied extensively during the last 5 decades,^{2,3} but studies that focus on the interplay between these two transitions are limited. Because of the slow kinetics associated with long-chain macromolecules, polymers are particularly well suited for this purpose, and the interplay of crystallization and LLPS in polymer blends has attracted much interest recently,^{4,5} due in part to the great practical importance of crystallizing polymer blends. Although most studies have focused on identifying the existence of LLPS through scattering measurements^{6–8} or morphological studies,^{8–10} the structures and dynamics that can arise from kinetic competition between LLPS and crystallization have received relatively limited attention, and several previous studies show that LLPS precedes crystallization in the unstable regime, with crystallization then occurring within the phase-separated medium.^{11–14} Although interesting morphologies and phenomenological models have been reported, a quantification of the ordering kinetics, particularly for critical blends within the unstable region of the phase diagram, is somewhat lacking. In this paper, we focus on the kinetics of closely conjugated solidification and phase separation in polyolefin blends. We observe a crossover from crystalliza-

tion dominated to phase-separation dominated kinetics, and we suggest, based on a scaling law for late-stage spinodal decomposition, that such a kinetic crossover is ubiquitous for blends in which the critical temperature of liquid–liquid phase separation is above the equilibrium melting temperature.

EXPERIMENT

The materials are statistical copolymers of ethylene/hexene (PEH) ($M_w = 110$ kg/mol, 2 mol % hexene comonomer) and ethylene/butene (PEB) ($M_w = 70$ kg/mol, 15 mol % butene comonomer).¹⁵ They are both synthesized with metallocene catalysts, and have relatively narrow polydispersity (~ 2) and uniform comonomer distribution.¹⁶ The phase diagram of the PEH/PEB blend has been determined previously¹⁶ and is shown in Fig. 1. The solid circles are measured LLPS temperatures at each composition, while the binodal and spinodal boundaries, shown as solid and dash lines, respectively, are calculated using Flory–Huggins formalism.¹⁶ The blend exhibits an upper critical solution temperature (UCST) at $T_{\text{cri}} = 146$ °C and $\phi_{\text{cri}} = 0.44$ in the melt. The open triangles are the measured equilibrium melting temperature, T_m^0 , as a function of composition,¹⁷ and the dotted line is a guide to the eye. The equilibrium melting temperature, T_m^0 , of PEH is 140 ± 3 °C,¹⁷ which is much higher than the melting temperature of PEB, ca. 40 °C, as measured by a single differential scanning calorimetry scan with a scan rate of 10 °C/min. In the scope of this study, PEB can be considered as an essentially amorphous component.

Equal amounts by mass of PEH and PEB were dissolved in a common xylene solution at ca. 100 °C and then coprecipitated by quenching into cold methanol at ca. 0 °C. After filtering, the polymers were dried in air for a day, and further dried in a vacuum oven at 100 °C for 3 days. Samples of a critical PEH/PEB blend, 50/50 by mass, denoted as H50, were hot-pressed between two glass plates at 160 °C to form films of ca. 20 μm thickness. For optical microscopy studies, the samples were kept in the melt at 160 °C for 5 min and

^{a)}Author to whom correspondence should be addressed. Electronic mail: hao.wang@nist.gov

^{b)}Permanent address: Department of Chemistry, Kyung Hee University, Kyungkido 449-701, South Korea.

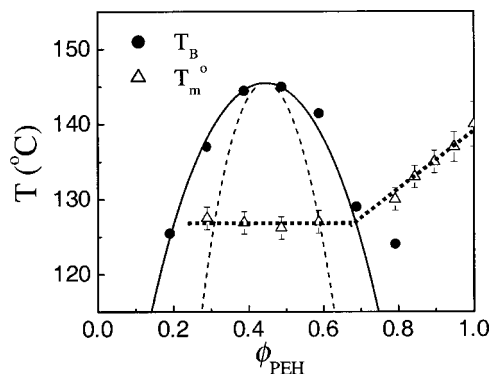


FIG. 1. Phase diagram of the PEH/PEB blend. The solid circles and the open triangles are measured values of liquid–liquid phase separation temperatures, T_B , and the equilibrium melting temperature, T_m^0 , respectively. The solid and dashed curves are calculated binodal and spinodal boundaries, respectively, and the dotted line is a guide to the eye. The phase diagram shows an upper critical solution temperature, $T_{crit}=146$ °C, and $\phi_{crit}=0.44$.

then quickly cooled down to the isothermal temperatures, T_c . Images of the crystallization were then recorded via bright-field illumination after various times at T_c . After isothermal storage and subsequent removal from the hot stage and cooling to room temperature in air, the samples were studied with small-angle light scattering (SALS) in both cross (H_v) and parallel-polarization (V_v) geometries.¹⁸ The scattering pattern was imaged on a screen behind the analyzer and recorded with a high resolution CCD camera, with a q -range spanning from 0.05 to $1.8 \mu\text{m}^{-1}$. Phase-contrast optical microscopy was used to image the LLPS morphology that evolves as a function of time after storing samples at 130 °C following melting at 160 °C. The variation of the isothermal temperature was within ± 0.2 °C.

RESULTS AND DISCUSSION

Figure 2 shows optical micrographs of the blend after isothermal crystallization (left column) for 10 min at 112 °C [Fig. 2(a)], 480 min at 115 °C [Fig. 2(c)], and 1200 min at 121 °C [Fig. 2(e)]. The samples were subsequently quenched to room temperature (right column) after 64 min at 112 °C [Fig. 2(b)], 960 min at 115 °C [Fig. 2(d)], and 1200 min at 121 °C [Fig. 2(f)]. The scale bar in the lower left corner is 20 μm . Figure 2(a) shows that spherulites grow and impinge upon each other, with crystallization being the dominant phase-ordering process. Upon cooling, radial features become less well defined due to further solidification of the segregated liquid phases. The light sheaflike features in Fig. 2(c) are early-stage spherulites that grow mostly during the first 60 min of the isothermal annealing. At a later time, crystal growth at that temperature is suppressed, and subsequent morphological change is mostly limited to the matrix region. This becomes more evident after quenching [Fig. 2(d)]. Proceeding higher, $T_c=121$ °C, small crystals (evident as white domains) are seen sparsely distributed within the sample after 1200 min [Fig. 2(e)]. Upon quenching to room temperature, the bicontinuous morphology due to LLPS becomes evident due to crystallization in the matrix [Fig. 2(f)].

The equilibrium melting temperature, T_m^0 , of H50 is 127 °C, as shown in Fig. 1.¹⁷ The degree of undercooling for

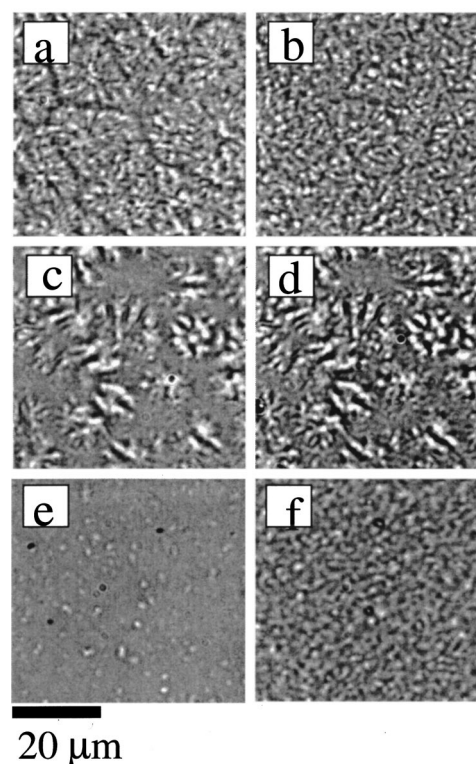


FIG. 2. Optical micrographs of H50 showing isothermal crystallization on the hot stage (left column) after 10 min at 112 °C (a), 480 min at 115 °C (c), and 1200 min at 121 °C (e), and after a quench to room temperature (right column) after 64 min at 112 °C (b), 960 min at 115 °C (d), and 1200 min at 121 °C (f). The scale bar at the bottom left is 20 μm .

isothermal crystallization at T_c is $\delta T=(T_m^0-T_c)/T_m^0$. For large undercooling, $T_c=112$ °C and $\delta T=0.0375$, crystallization clearly dominates the morphological development. For $T_c=115$ °C and $\delta T=0.03$, crystallization is prominent at the early times when the blend is relatively homogeneous in composition. As crystals grow, liquid–liquid phase separation proceeds in the matrix, resulting in a composition variation that is larger in both wavelength and amplitude. The high barrier of the depleted region due to composition inhomogeneity prohibits incipient spherulites from maturing into spherical shapes. Similar cessation of spherulitic growth in a phase-separating medium has been reported previously.¹⁹ Further crystallization occurs within phase-separated, bicontinuous tubes. Due to the nearly identical refractive indices of the two polymer components in the melt, the LLPS morphology is not readily observed with bright-field optical microscopy at elevated temperatures. At small undercooling ($T_c=121$ °C and $\delta T=0.015$), crystallization proceeds very slowly, and the growth of phase-separated domains is the faster process. Crystallization is thus mainly confined to the PEH-rich regions of the already established liquid–liquid separated domains. After quenching, the crystallizable component in both of the coexisting liquid phases crystallizes, resulting in markedly different refractive indices and significant optical contrast between the two phases.

The observations in real space are also verified in reciprocal space by SALS. Figure 3 shows the cross-polarized

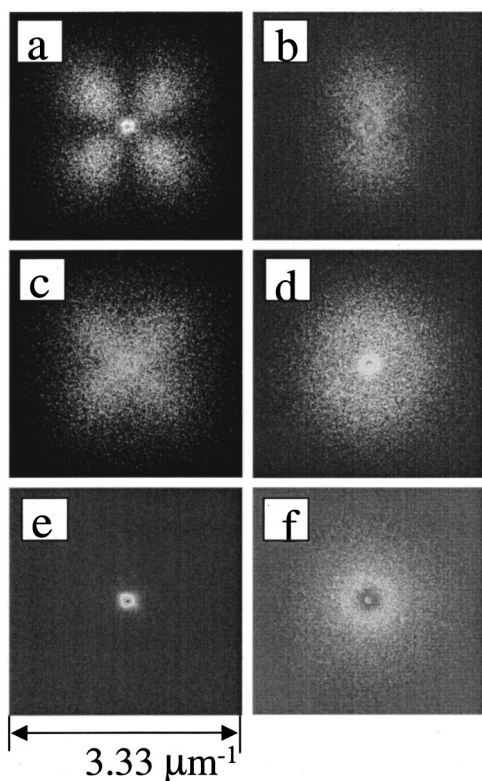


FIG. 3. The H_v (left) and V_v (right) small-angle light scattering patterns of the H50 blend after annealing at 112 °C (a) and (b), 115 °C (c) and (d), and 121 °C (e) and (f) and subsequently quenching to room temperature. The width of each scattering pattern is $3.33 \mu\text{m}^{-1}$.

(H_v) (left column) and parallel-polarized (V_v) (right column) light scattering pattern for the H50 blend after isothermal crystallization at 112 °C (a) and (b), 115 °C (c) and (d), and 121 °C (e) and (f) and subsequent quenching to room temperature. The fourfold symmetry in the H_v pattern [Fig. 3(a)] and the twofold symmetry in V_v pattern [Fig. 3(b)] indicate well-defined spherulites grown at 112 °C [Fig. 2(a)]. The H_v pattern at 121 °C shows little scattering [Fig. 3(e)], suggesting a lack of spherulitic ordering, whereas the isotropic V_v pattern [Fig. 3(f)] indicates that liquid–liquid phase separation dominates the morphological development. These represent two extremes for crystallization dominated and phase-separation dominated behaviors, respectively. For $T_c = 115 \text{ °C}$, the H_v pattern is very diffuse [Fig. 3(c)], suggesting only weak spherulitic ordering; whereas the V_v pattern shows a mixture of a twofold spherulitic symmetry and an isotropic spinodal ring [Fig. 3(d)], consistent with the morphology shown in Fig. 2(d).

Previously, optical contrast resulting from crystallization in the segregated liquid phases has been employed to measure the phase diagram.¹⁶ This indirect technique provides a quick and sensitive determination of the phase boundary, but it is not sufficient for a measurement of the LLPS kinetics, which requires a direct probe of the liquid–liquid domains. Figure 4 shows phase-contrast optical micrographs of the H50 blend stored at 130 °C for (a) 135 min, (b) 255 min, (c) 495 min, and (d) 1035 min, respectively. Spinodal decomposition is evident as bicontinuous, interconnected PEH-rich and PEH-poor phases that coarsen with time. The character-

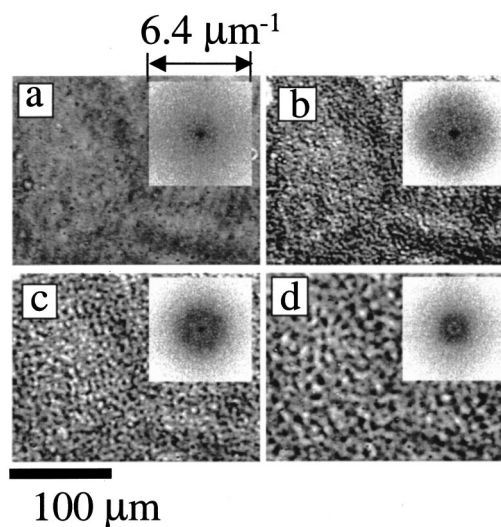


FIG. 4. Phase-contrast optical micrographs of the H50 blend after annealing at 130 °C for (a) 135 min, (b) 255 min, (c) 495 min, and (d) 1035 min. Bicontinuous, interconnected PEH-rich and PEH-poor phases are evident as light and dark domains that coarsen with time. The scale bar at the bottom left is $100 \mu\text{m}$.

istic length scale, $l(t)$, for the phase-separation process is obtained from these images *via* a fast-Fourier-transform (FFT) analysis. The 2D FFT images are shown as insets in Fig. 4. Radially averaged profiles give the predominant wave vector, q_m , with $l = 2\pi/q_m$, which grows linearly with time, $l \propto t$ (see inset of Fig. 6). We should emphasize that the small optical contrast between PEH and PEB limits this analysis to relatively late times, where the LLPS domains are relatively large and well defined.

As an approximation, crystallization and phase separation can be considered as independent processes. The early-stage kinetics of spinodal decomposition first described by Cahn and Hilliard²⁰ is not the main concern in the current study. Rather, late-stage spinodal decomposition, where hydrodynamic forces drive the coarsening,²¹ is the relevant growth process. In this late-stage regime, the phase-coarsening kinetics follows the simple growth law:

$$l \propto \frac{\sigma}{\eta} t, \quad (1)$$

where σ and η are the interfacial tension between the coexisting phases and the effective viscosity of the fluid, respectively, and t is the time following a quench into the unstable region of the phase diagram. For a critical binary fluid, dimensional analysis suggests

$$\sigma \propto \frac{k_B T}{\xi^{d-1}}, \quad (2)$$

where k_B is the Boltzmann constant, $d=3$ is the spatial dimension, and ξ is the thermal correlation length. The temperature dependence of the correlation length, $\xi = [(T_{\text{cri}} - T)/T_{\text{cri}}]^{-\nu}$, leads to a surface tension, σ , that roughly scales as $[(T_{\text{cri}} - T)/T_{\text{cri}}]^{(d-1)\nu}$. For high-molecular-weight polymer mixtures far from the critical point, the exponent ν is approximately 0.5.² If the viscosities of the two components are similar and the temperature range of interest is

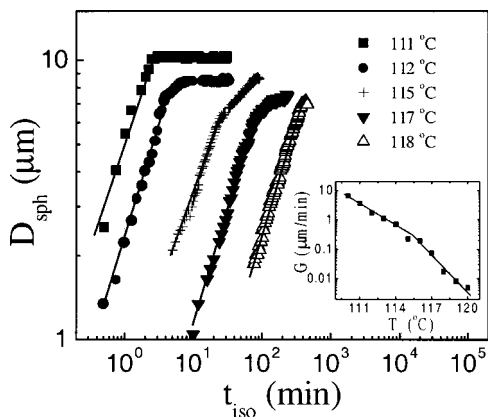


FIG. 5. Time evolution of the average spherulite diameter at various isothermal crystallization temperatures for the H50 blend. Linear growth at early times is observed for all temperatures. The inset shows the linear growth rate as a function of the isothermal annealing temperature, indicating a crossover in the growth mechanism at around 115 °C.

small (on an absolute scale) and well above the glass transition temperatures ($T_g \approx -40$ °C), η can be approximated as a constant, and the growth rate of the liquid phases is

$$l' \approx l/t \propto (T_{\text{cri}} - T)/T_{\text{cri}}. \quad (3)$$

As described above, the crystallization kinetics can be measured using bright-field optical microscopy. Figure 5 shows a log–log plot of the time evolution of the average spherulite diameter, D_{sph} , in the H50 blend for various isothermal crystallization temperatures. Initially, the spherulites grow linearly with time because the melt is mostly homogeneous, and a semilogarithmic plot of early-time linear growth rate, G , for each temperature is shown in the inset. A kink in $\log G(T_c)$ separates a high-temperature regime (regime I) and a low-temperature regime (regime II), indicating a crossover in the crystallization kinetics.²²

The crystal growth rate depends on the crystallization mechanism. In regime I, single crystal nucleation at a crystal surface causes layer-by-layer growth, whereas in regime II, because of the large secondary nucleation rate at high undercooling, multiple nuclei exist on the same crystallization surface. A unified formalism gives the growth rate as

$$G_i = k_i e^{Q_D^*/RT_c} e^{-K_{g,i}/(T_c^* \Delta T)}, \quad (4)$$

where the subscript i denotes I or II (for regime I or II), ΔT is the difference between $T_m^0 = 127$ °C and T_c , k and R are molecular and thermal constants, respectively, Q_D^* is the activation energy for steady-state reptation, and K_g is the nucleation constant.²² By fitting the data in Fig. 5, $K_{g,I}$ and $K_{g,II}$ are found to be $(1.3 \pm 0.2) \times 10^5$ K² and $(1.1 \pm 0.1) \times 10^5$ K², respectively, suggesting that the approximate relationship $K_{g,I} \approx 2K_{g,II}$ (Ref. 22) does not apply to crystallization in the blend under consideration. The uncertainty in T_m^0 does not alter either the regime assignment or the K_g relationship.

Based on the above arguments, the growth rates of the two ordering processes are shown in Fig. 6. The solid and dashed lines depict the rate of crystal superstructure growth and phase coarsening, respectively. The crystallization

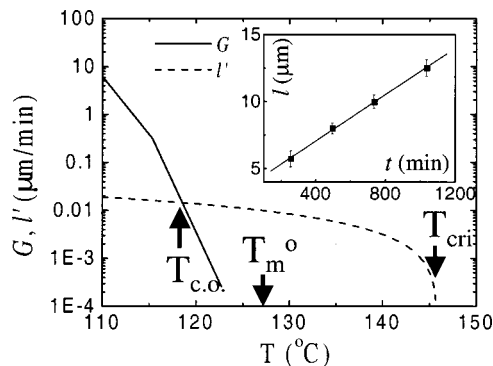


FIG. 6. A comparison of growth rates for LLPS and crystallization as a function of quench depth. The inset shows the characteristic length scale of the LLPS as a function of time, for which a linear fit gives the constant of proportionality in the scaling law. The critical temperature (T_{cri}), the equilibrium melting temperature (T_m^0), and the kinetic crossover temperature (T_{co}) are all indicated by arrows.

growth rate is the measured value depicted in Fig. 5, while the growth rate for phase separation is estimated from the scaling law described above, with the coefficient of proportionality given by fitting the measured $l(t)$ at 130 °C, as shown in the inset of Fig. 6. Using the proportionality constant of 0.1 in the Eq. (1) as suggested by Siggia in his original paper,²¹ an average zero-shear viscosity of 10^5 Pa s for the blend at 130 °C, and a typical interfacial tension of 0.1 mN/m for polyolefins, the growth rate l' for phase coarsening is estimated to be 10^{-4} μm/s, consistent with that shown in Fig. 6. The crystallization growth rate varies dramatically over a temperature window of 20 K below T_m^0 , and diminishes near T_m^0 of the H50 blend. On the other hand, the implied variation in the phase-separation kinetics over the same temperature range is much less dramatic, although it rapidly diminishes near criticality. Interestingly, the crossover temperature suggested by these qualitative physical arguments ($T_{\text{co}} \approx 118$ °C) is consistent with the experimental observations. It is obvious from Fig. 6 that such a kinetic crossover is ubiquitous for blends in which the critical temperature of liquid–liquid phase separation is above the equilibrium melting temperature.

At very early time upon quenching a homogeneous blend into a regime of simultaneous spinodal decomposition and crystallization, the former dominates because the composition fluctuations are inherently unstable, and the growth process does not require overcoming an energy barrier, as is always the case for crystallization.²³ In this paper, however, we discuss mainly the competition between the development of crystal superstructure and late-stage phase coarsening. In other words, we compare length scales of crystals and phase-separated liquid domains at late stages of development.

The phenomenological argument given above is rather simple and straightforward. The microscopic picture, however, can be more complicated. During simultaneous LLPS and crystallization, the crystal front is a zone that is depleted in the crystallizable species and rich in the noncrystallizable ones, which include most of the PEB polymer and side-chain-enriched PEH. At large undercooling, crystals grow

very fast by taking in the short polyethylene segments while expelling the noncrystallizable chains in the interlamellar stack region. Crystal growth sweeps through the phase separating medium, including the PEB rich regions, and fills the entire volume, resulting in a spherulitic-growth dominated morphology. At smaller undercoolings, more PEH chain segments become noncrystallizable, and slower crystallization allows the ejection of the noncrystallizable component outside of the lamellar stacks, further widening the depletion zone at the crystal front. With both a decrease in the driving force and an increase in the energetic barrier for chains to diffuse across the depletion zone, the spherulites can cease to grow at later times, with further crystallization occurring mainly in PEH-rich domains of the phase-separated matrix. At even smaller undercoolings, crystallization involves only a very small portion of the chains, and the slow kinetics and limited crystallinity allow LLPS to develop.

The above picture is very different from a previous morphology study on the interplay between liquid demixing and crystallization in polypropylene and ethylene-propylene copolymer mixture.²⁴ In that study, the main focus was on crystallization in phase separated blends that were not initially in a thermodynamically miscible state; furthermore, only crystals arresting liquid coarsening occurred, not the other way around. A phenomenologically relevant study shows that in dual crystallization and phase separation in binary colloidal mixtures following a single quench, phase separation is the prerequisite for crystallization.²⁵ We should also point out that the shape of the growth rate curve for LLPS will deviate dramatically from that shown in Fig. 6 for temperatures below the crossover point, since the hydrodynamics of the liquid phase coarsening will be drastically altered by the onset of crystalline order. This effect is apparent in Figs. 2(e) and 2(f), where kinetic trapping for crystallization and phase separation is mutual, as the morphology that develops from each process limits the growth of the other. From another perspective, the rheological consequences of crystallization can be compared to a gelation transition²⁶ and vitrification²⁷ of the fluid dynamics.

CONCLUSION

By combining real-space observation and small-angle light scattering, we have shown that in a simultaneously crystallizing and phase separating polymer blend, after an initial transient stage, the morphology development exhibits a crossover from crystal superstructure dominated to liquid phase-coarsening dominated behavior based on the relative quench depth for the two ordering processes. The corresponding morphology is volume-filling spherulites for the former and bicontinuous, interconnected tubes for the latter. This crossover, which is observed experimentally, is shown to be inevitable based on a simple scaling argument for uncoupled late-stage spinodal decomposition and crystallization. This simple argument, however, does not account for the complexity involved in the crystallization of short-chain

branched polymers, which is conceptually different from model colloidal mixtures or small-molecule systems, and it does not account for coupling between the two processes associated with dramatic rheological changes in the coarsening LLPS domains upon crystallization.

ACKNOWLEDGMENT

The authors acknowledge critical comments by Freddy A. Khoury (NIST) and Stephen Z. D. Cheng (Akron).

- ¹E. Di Marzio, *Prog. Polym. Sci.* **24**, 329 (1999).
- ²P. G. de Gennes, *Scaling Concepts in Polymer Physics* (Cornell University Press, New York, 1979).
- ³B. Wunderlich, *Macromolecular Physics* (Academic, New York, 1973).
- ⁴B. Crist and M. J. Hill, *J. Polym. Sci., Polym. Phys. Ed.* **35**, 2329 (1997).
- ⁵L. Mandelkern, R. G. Alamo, G. D. Wignall, and E. C. Stehlin, *Trends Polym. Sci.* **4**, 377 (1996).
- ⁶N. P. Balsara, L. J. Fetters, N. Hadjichristidis, D. J. Lohse, C. C. Han, W. W. Graessley, and R. Krishnamoorti, *Macromolecules* **25**, 6137 (1992).
- ⁷J. Rhee and B. Crist, *J. Chem. Phys.* **98**, 4174 (1993).
- ⁸R. Briber and F. Khoury, *Polymer* **28**, 38 (1987); *J. Polym. Sci., Polym. Phys. Ed.* **31**, 1253 (1993).
- ⁹P. J. Barham, M. J. Hill, A. Keller, and C. C. A. Rosney, *J. Mater. Sci. Lett.* **7**, 1271 (1998).
- ¹⁰M. J. Hill, P. J. Barham, A. Keller, and C. C. A. Rosney, *Polymer* **32**, 1384 (1991).
- ¹¹H. Tanaka and T. Nishi, *Phys. Rev. Lett.* **55**, 1102 (1985); *Phys. Rev. A* **39**, 783 (1989).
- ¹²P. M. Cham, T. H. Lee, and H. Marand, *Macromolecules* **27**, 4263 (1994).
- ¹³I. Isayeva, T. Kyu, and R. J. Manley, *Polymer* **39**, 4599 (1998).
- ¹⁴V. Ferreiro, J. F. Douglas, E. J. Amis, and A. Karim, *Macromol. Symp.* **167**, 73 (2001).
- ¹⁵Certain equipment, instruments or materials are identified in the paper in order to adequately specify the experimental details. Such identification does not imply recommendation by the National Institute of Standards and Technology, nor does it imply the materials are necessarily the best available for the purpose.
- ¹⁶H. Wang *et al.*, *Macromolecules* **35**, 1072 (2002).
- ¹⁷The T_m^0 is determined following Hoffman-Weeks approach over a limited range, and may be overestimated for PEH and blends (Ref. 16). The robustness of this approach has been questioned recently [H. Marand *et al.*, *Macromolecules* **31**, 8219 (1998)] and its applicability to statistical copolymers has been discussed. However, T_m^0 still provides a good reference for thermodynamic considerations in polymer crystallization. More importantly, the absolute value of T_m^0 does not alter the physical picture and the conclusion of the current study.
- ¹⁸R. S. Stein and M. B. Rhode, *J. Appl. Phys.* **31**, 1873 (1960).
- ¹⁹H. Wang and C. C. Han, *Polym. Prepr. (Am. Chem. Soc. Div. Polym. Chem.)* **42**, 1844 (2000).
- ²⁰J. W. Cahn and J. E. Hilliard, *J. Chem. Phys.* **28**, 258 (1958); **31**, 688 (1959); *J. W. Cahn, Acta Metall.* **9**, 795 (1961); *J. Chem. Phys.* **42**, 93 (1965).
- ²¹L. P. McMaster, *Adv. Chem. Ser.* **142**, 43 (1975); E. D. Siggia, *Phys. Rev. A* **20**, 595 (1979); T. Koga and K. Kawasaki, *ibid.* **44**, R817 (1991); S. Puri and B. Dunweg, *ibid.* **45**, R6977 (1992).
- ²²J. D. Hoffman, G. T. Davis, and J. I. Lauritzen, in *Treatise on Solid State Chemistry, V3; Crystalline and Non-crystalline Solids*, edited by N. B. Hannay (Plenum, New York, 1976).
- ²³A. Keller and S. Z. D. Cheng, *Polymer* **39**, 4461 (1998); S. Z. D. Cheng and A. Keller, *Annu. Rev. Mater. Sci.* **28**, 533 (1998).
- ²⁴N. Inaba, K. Sato, S. Suzuki, and T. Hashimoto, *Macromolecules* **19**, 1690 (1986); N. Inaba, K. Yamada, S. Suzuki, and T. Hashimoto, *ibid.* **21**, 407 (1988).
- ²⁵E. K. Hobbie, *Phys. Rev. Lett.* **81**, 3996 (1998).
- ²⁶N. V. Pogodina and H. H. Winter, *Macromolecules* **31**, 8164 (1998).
- ²⁷J. Arnouts and H. Berghmans, *Polym. Commun.* **28**, 66 (1987).